Solar Energy 153 (2017) 383–395

Contents lists available at ScienceDirect

Solar Energy

journal homepage: www.elsevier.com/locate/solener

Thermal performance analysis of an inclined passive solar still using agricultural drainage water and artificial neural network in arid climate

Ahmed F. Mashaly [a,*], A.A. Alazba [a,b]

[a] Alamoudi Water Research Chair, King Saud University, Riyadh, Saudi Arabia
[b] Agricultural Engineering Department, King Saud University, Riyadh, Saudi Arabia

ARTICLE INFO

Article history:
Received 1 December 2015
Received in revised form 12 April 2017
Accepted 28 May 2017

Keywords:
Artificial neural network
Thermal efficiency
Solar still
Multiple linear regression
Agricultural drainage water

ABSTRACT

In this study, a model based on artificial neural network (ANN) was developed in order to predict the thermal performance of an inclined passive solar still in an arid climate, in which the thermal performance of the still was expressed as instantaneous thermal efficiency (ITE). Agricultural drainage water (AWD) was used as a feed for the desalination process, and this is considered a non-conventional water source. Appropriate meteorological variables, viz., ambient air temperature, relative humidity, wind speed, and solar radiation were used alongside the key operational variables, viz., flow rate, temperature, and total dissolved solids of feed water were used as input variables. The results revealed that an ANN with six neurons and a hyperbolic tangent transfer function was the most appropriate model for ITE prediction. Consequently, the optimal ANN model had a 7–6–1 architecture. The results also indicated that the optimal ANN model forecast the ITE accurately, with a mean root mean square error (RMSE) of just 1.933% and a mean coefficient of determination (CD) of 0.949. To create a sensible comparison, a multiple linear regression (MLR) model was also developed. It was found that the ANN model performed better than the MLR model, which displayed a mean RMSE of 4.345% and a mean CD of 0.739. The mean relative errors of forecasted ITE values within the ANN model were mostly in the region of +8% to −6%. One major output of this research is a comprehensive assessment of the ANN modeling technique for the ITE of a solar still, which adds a new perspective to system analysis, design and modeling of the potential productivity of solar stills in terms of the AWD desalination process.

1. Introduction

Globally, water consumption is dominated by agricultural activities, especially irrigation which account for 70% of consumption (WWAP, 2014), while approximately two-thirds of the water delivered to irrigated fields is lost as agricultural drainage or runoff (Gregory, 2012). However, the availability of plenty of agricultural drainage water (ADW) creates promising opportunities for desalinating significant quantities of water from this non-conventional source. The selection process of the appropriate method for desalinating this source is challenged by numerous technical, financial, and environmental issues to be taken into account (Sorour et al., 2003). Most published studies and research consider conventional desalination methods operated by fossil fuel energy or electrical energy for AWD desalination (Sorour et al., 1992; Abulnour et al., 2003; Talaat and Ahmed, 2007; McCool et al., 2010). Recently, some studies have proposed using solar energy for the AWD desalination process (Stuber et al., 2015; Mashaly et al., 2015a).

The solar still desalination system (SSDS) for AWD is a strategic option that can be used for producing fresh water suitable for agricultural, irrigation, and potable purposes (Mashaly et al., 2015b) and reducing the drainage water volume, which would minimize the environmental problems associated with it. Moreover, the SSDS exploits a sustainable and pollution-free source to yield high-quality water (Ayoub and Malaeb, 2012) and is one of the best solutions for facing water crises in remote arid and hyper-arid environments. It can be fabricated without difficulty with locally available materials and its operation is simple and easy, with no need for hard maintenance or skilled labor. This results in little operation and maintenance costs (Omara and Kabeel, 2014).

On the other hand, the SSDS is not popular because of its lower thermal performance and this is reflected in its efficiency. Of course, this will cause fear and hesitation for many people considering using it in the AWD desalination process. Thus, thermal performance analysis for the SSDS is very important. This enables us to know the thermal capacity of the SSDS and its potential productivity

* Corresponding author.
E-mail addresses: amashaly@ksu.edu.sa, mashaly.ahmed@gmail.com (A.F. Mashaly).

http://dx.doi.org/10.1016/j.solener.2017.05.083
0038-092X/

Nomenclature

ADW	agricultural drainage water
ANN	artificial neural network
AS	area of solar still
AVG	average value
B_j	biases in the hidden layer
B_k	biases in the output layer
BP	back propagation
CC	correlation coefficient
CD	coefficient of determination
CRM	coefficient of residual mass
CS	Chi-square
CV	coefficient of variation
F_h	activation function of the neuron in the output layer
F_o	activation function of the neurons in the hidden layer
ITE	instantaneous thermal efficiency
KPIs	key Performance Indicators
KUR	kurtosis value
LHV	latent heat of vaporization
MAE	mean absolute error
MAX	maximum value
ME	coefficient of model efficiency
M_F	feed flow rate
MIN	minimum value
MLP	multilayer perceptron
MLR	multiple linear regression
MXE	maximum error
OI	overall index of model performance
RH	relative humidity
RMSE	root mean square error
SD	standard deviation
SE	standard error
SIG	sigmoid transfer function
SKW	Skewness value
SR	solar radiation
SSDS	solar still desalination system
TANH	hyperbolic tangent transfer function
TDS_F	total dissolved solids of feed water
T_F	temperature of feed water
T_o	ambient temperature
W_{ji}	weights between input and hidden layers
W_{kj}	weights between hidden and output layers
WS	wind speed

and thermal efficiency. Actually, the precise and detailed thermal performance of the SSDS is quite complicated because of the many parameters involved, as its operation is governed by many heat transfer processes (Shukla, 2014). Consequently, efforts should be made to combine a number of the most vital parameters into an algebraic expression and formulate a mathematical model that can describe the thermal performance of the SSDS in a computationally efficient manner.

The question is how to model the thermal performance (i.e. the useful energy gain or the solar still thermal efficiency). Compared with classical modeling procedures, artificial neural networks (ANNs) show superiority as a modeling procedure for data sets presenting non-linear relationships and thus for both data-fitting and prediction capabilities (Bourquin et al., 1998). ANNs are non-linear models that mimic the learning process of the human brain, as the equations that can most efficiently diminish the gap between predicted data and observed data are chosen iteratively (Goh, 1995). They can be a powerful tool for predicting, optimizing and simulating complex nonlinear processes (Lek and Guégan, 1999; Basheer and Hajmeer, 2000; Fadare, 2009). Thermal solar energy systems can be precisely modeled using ANNs (Kalogirou et al., 1999a). Several studies have presented the applications of ANNs in the field of solar energy applications for various agricultural activities (Ferreira et al., 2002; Tripathy and Kumar, 2009; Çakmak and Yildiz, 2011; Arif et al., 2012; Dursun and Özden, 2014). Furthermore, ANNs have been widely employed in multiple ways to model, optimize, estimate, and forecast the performance of various desalination and solar desalination systems (Abbas and Al-Bastaki, 2005; Khayet et al., 2011; Porrazzo et al., 2013; Mashaly et al., 2015c; Aish et al., 2015; Mashaly and Alazba, 2016a, 2016b, 2016c; Cao et al., 2016; Mashaly and Alazba, 2017).

However, most of the existing/previous research on the SSDS has focused on modifying the solar still design configuration to enhance and improve the thermal efficiency, productivity, and performance of the still (Rai and Tiwari, 1983; Singh and Tiwari, 2004; Tripathi and Tiwari, 2005; Tiwari and Tiwari, 2006; Velmurugan et al., 2009; Monowe et al., 2011; Abderachid and Abdenacer, 2013; Refalo et al., 2016; Sharon et al., 2017). On the other hand, SSDS should be optimally designed and operated, and predictive modeling of thermal efficiency is one of the crucial parameters to be precisely estimated since it helps us to know the potential efficiency attainable by the SSDS and to ensure obtaining the best performance and optimal productivity and efficiency. To our knowledge, there has been no previous research directly examined and focused on determining the effectiveness of modeling thermal efficiency of SSDS desalinated AWD using ANNs. In the current study, we are planning to take a step towards this objective by implementing, developing and analyzing an ANN model for estimating thermal efficiency, which was expressed here as instantaneous thermal efficiency (ITE). The aims of this study are to (1) develop a mathematical model to estimate the ITE using ANNs; (2) assess and analyzes the performance of the developed ANN model by comparing the ITE results obtained from the ANN and the experimental results statistically; (3) compare the ANN model with multiple linear regression (MLR) model in terms of their appropriateness and accuracy for predicting ITE; and (4) determine the importance or contribution of each variable in modeling process.

2. Materials and methods

2.1. Experimental set-up

The experiments were conducted at the Agricultural Research and Experiment Station at the Department of Agricultural Engineering, King Saud University, Riyadh, Saudi Arabia (24°44′10.90″ N, 46°37′13.77″E) between October and November 2013. The weather data were obtained from a weather station (model: Vantage Pro2; manufacturer: Davis, USA) close by the experimental site (24°44′12.15″N, 46°37′14.97″E). The solar still system used in the experiments was constructed from a 6 m^2 single stage C6000 panel (F Cubed. Ltd., Carocell Solar Panel, Australia). The solar still panel was manufactured using modern, cost-effective materials such as coated polycarbonate plastic. When heated, the panel distilled a film of water that flowed over the absorber mat of the panel. The panel was fixed at angle of 29° from the horizontal plane. The basic construction materials were galvanized steel legs, an aluminum frame and polycarbonate covers. The transparent polycarbonate was coated on the inside with a special material

to prevent fogging (patented by F Cubed- Australia). Photo and cross-sectional view of the inclined solar still are presented in Fig. 1.

The water was fed to the panel using centrifugal pump (model: PKm 60, 0.5 HP, Pedrollo, Italy) with a constant flow rate was 10.74 L/h. A manually operated discharge valve was fitted after the pump serves to decrease the flow so that this flow rate is achieved. A screen filter was fitted just before the pump. The feed was supplied by eight drippers/nozzles, creating a film of water that flowed over the absorbent mat. Underneath the absorbent mat was an aluminum screen that helps to distribute the water across the mat. Beneath the aluminum screen was an aluminum plate. Aluminum was chosen for its hydrophilic properties, to assist in the even distribution of the sprayed water. Water flows through and over the absorbent mat, and solar energy was absorbed and partially collected inside the panel; as a result, the water is heated and hot air circulated naturally within the panel. First, the hot air flowed toward the top of the panel, and then reversed its direction to approach the bottom of the panel. During this process of circulation, the humid air touches the cooled surfaces of the transparent polycarbonate cover and the bottom polycarbonate layer, causing condensation. The condensed water flowed down the panel and was collected in the form of a distilled stream. Agricultural drainage water (AWD) was used as a feed water input to the system. The solar still system was run from 10/05/2013 to 11/01/2013. Raw AWD was obtained from Al-Oyun City, Al-Ahsa, in eastern

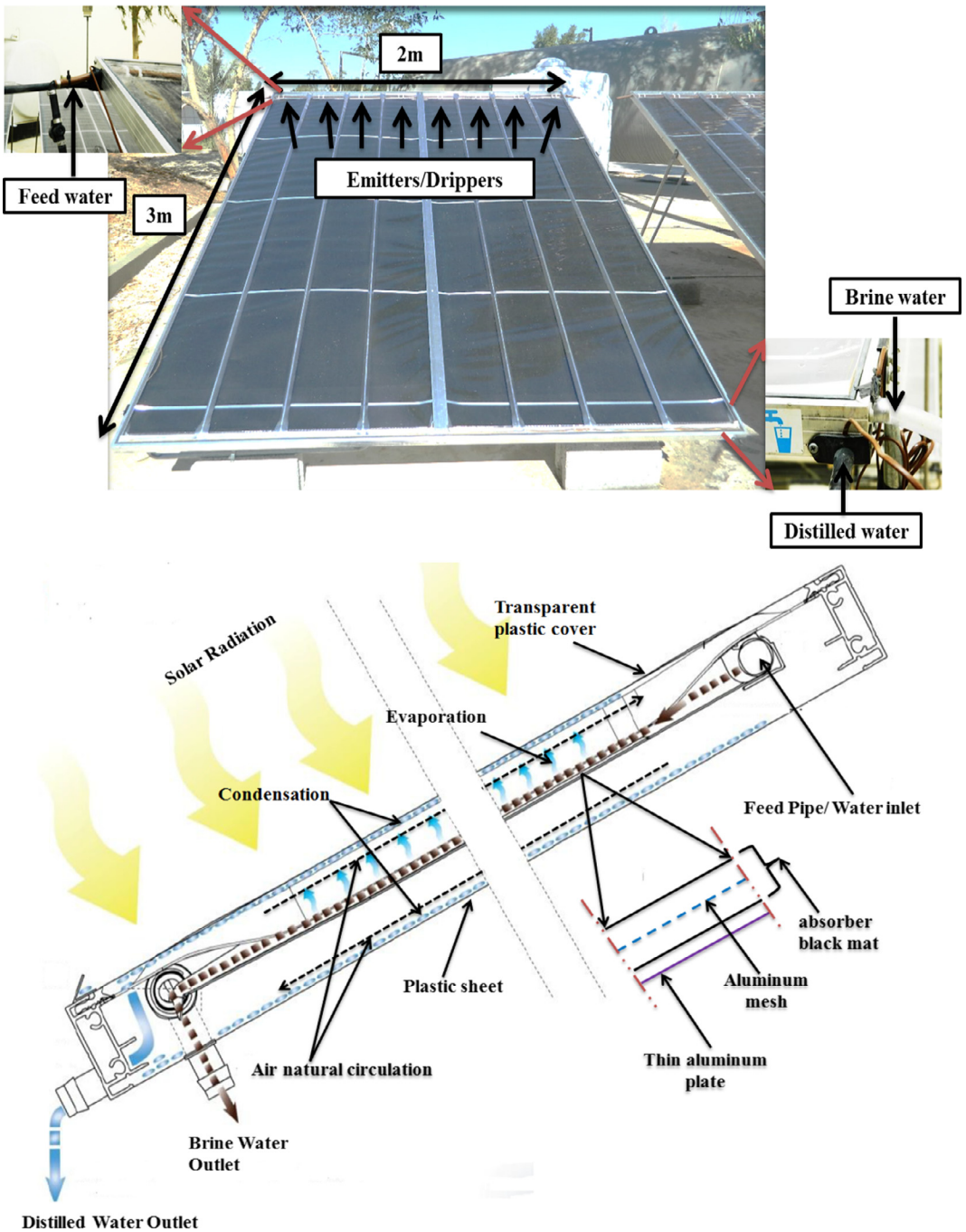

Fig. 1. Photo and cross-sectional view of the inclined solar still.

Saudi Arabia (25°35′7.02″N, 49°35′48.17″E). The initial concentrations of total dissolved solids (TDS), pH, density (ρ) and electrical conductivity (EC) of the raw AWD were 4.71 ppt, 8.1, 1.001 g cm^{-3}, and 7.54 mS cm^{-1}, respectively. The temperature of the feed water (T_F) was measured by using thermocouples (T-type, UK). The T_F was recorded on a data logger (model: 177-T4, Testo, Inc., UK) at 1 min intervals. The amount of feed water (M_F) was measured by calibrated digital flow meter was mounted on the feed water line (micro-flo, Blue-White, USA). The amount of brine water and distilled water were measured by a graduated cylinder. TDS concentration and EC were measured using a TDS-calibrated meter (Cole-Parmer Instrument Co. Ltd., Vernon Hills, USA). A pH meter (model: 3510 pH meter; Jenway, UK) was used to measure pH. A digital-density meter (model: DMA 35N, Anton Paar, USA) was used to measure ρ. The AWD was fed separately to the panel using the pump described above. The residence time—the time taken for the water to pass through the panel—was approximately 20 min. Therefore, the flow rate of the feed water, the distilled water and the brine water was measured every 20 min. Also, the total dissolved solids of feed water (TDS_F) were measured every 20 min. The weather data, such as air temperature (T_o), relative humidity (RH), wind speed (WS) and solar radiation (SR), were obtained from a weather station near the experimental site.

2.2. Computation of instantaneous thermal efficiency (ITE)

The ITE is a form of thermal efficiency of solar still which is defined as the ratio of the amount of thermal energy utilized to get a certain amount of distilled water to the instantaneous incident solar radiation. The mathematical expression used to calculate ITE can be written using the following formula (Tiwari, 2006; Badran and Abu-Khader, 2007):

$$ITE = \frac{\dot{M}D \times LHV}{SR \times AS} \quad (1)$$

where $\dot{M}D$ is the mass flow rate of distilled water, kg/s

LHV: Latent heat of vaporization = 2275 kJ/kg
SR: Solar radiation on tilted surface, kW/m^2
AS: Area of solar still, m^2.

2.3. ANN modeling methodology

ANN is an enormously parallel distributed information-processing system that can store the experiential knowledge acquired by the process of learning, and of making it accessible for future use (Haykin, 1999). In this study, the feed forward multilayer perceptron (MLP) with back-propagation (BP) learning rule was used, which is the most commonly used ANN architecture in thermal modeling and solar desalination (Kalogirou, 2006; Benli, 2013; Mashaly and Alazba, 2015). The architecture of the ANN model used is displayed in Fig. 2. The ANN model consists of the input layer (i), one hidden layer (j) and an output layer (k) as indicated. The i layer is connected to the j layer and in turn the j layer is connected to the k layer by connection weights (W). Each of j layer and k layer has an additional element called a bias (B). The j layer neurons contain activation functions, which assist in translating the input variables to the output variable (ITE). As the output of the MLP network, the ITE was computed as (Haykin, 1999):

$$ITE = F_o\left\{B_k + \sum_{j=1}^{m}\left[W_{kj}F_h\left(B_j + \sum_{i=1}^{n}W_{ji}X_i\right)\right]\right\} \quad (2)$$

where B_k is the bias at the output layer; W_{kj} is the weight of connection between the node j of the hidden layer and the single output layer neuron; B_j is the bias at the neuron j of the hidden layer (j = 1,2, . . . ,n); W_{ji} is the weight of connection between input variable i (i = 1,2, . . . , m) and neuron j of the hidden layer; X_i is the input variable (T_o, RH, WS, SR, T_F, TDS_F and M_F); F_o is the activation function of the neurons in the hidden layer; and F_h is the activation function of the neuron in the output layer. Different transfer functions in hidden and output layers with different number of nodes in the hidden layers were investigated, namely; sigmoid transfer function (SIG) and hyperbolic tangent transfer function (TANH). SIG for any variable Z is expressed as:

$$F(Z) = \frac{1}{1 + \exp(-Z)} \quad (3)$$

Also, TANH for any variable Z is expressed as:

$$F(Z) = \frac{1 - \exp(-2Z)}{1 + \exp(-2Z)} \quad (4)$$

In the present study, the ITE of the solar still system was the output variable, and nd T_o, RH, WS, SR, TDS_F, M_F, and T_F, were the input variables. The modeling process comprised the training, testing, and validation periods. Therefore, the experimental data were divided into three datasets for the aforementioned periods. The first dataset was used to train the network (training period), the second dataset was used to test the ANN models for defining the termination point of the training process (testing period), and the third dataset was used to validate the data on ANN models that were not included in the training period (validation period). The available dataset comprising which consists of 56 data points obtained from the experimental study was randomly divided into training (n = 39, 70%), testing (n = 11, 20%) and validation (n = 6, 10%) subsets. For predicting the thermal performance of a solar water heater, Kalogirou et al. (1999b) used 54 data points to successfully develop an ANN model. The results indicated that these data points were sufficient for developing an effective and precise ANN model. In the present study, the ANN model was developed using Qnet2000. Before the modeling process, the data were automatically normalized between 0.15 and 0.85 by using Qnet2000. This data normalization accelerated the training process and enhanced network's generalization capabilities. The following mathematical equation was used for the normalization process:

$$X_n = \left(\frac{X_o - X_{\min}}{X_{\max} - X_{\min}}\right) \times (0.85 - 0.15) + 0.15 \quad (5)$$

where X_n is the normalized value; X_o is the original value of input and output variables; and X_{max} and X_{min} are the maximum and minimum values of input and output variables, respectively.

The main aim of a model development process is to determine an optimal network architecture that can yield prediction results for ITE with acceptable accuracy levels. The optimal number of hidden nodes and most favorable transfer function should be determined. In order to archive that, different architectures are obtained by increasing the number of hidden nodes in the ANN model. These architectures are trained, checked and tested. The training process is conducted with the two transfer functions (SIG and TANH) for each architecture to compare the performance and find the best function. The training was carried out iteratively and was terminated when the error falls below acceptable level or when it reaches the maximum number of iterations. By trial and error, the maximum number of training iterations is set to be 50,000. At the end, comparison is conducted among the different architectures based on statistical numerical indicators to find the most appropriate ANN.

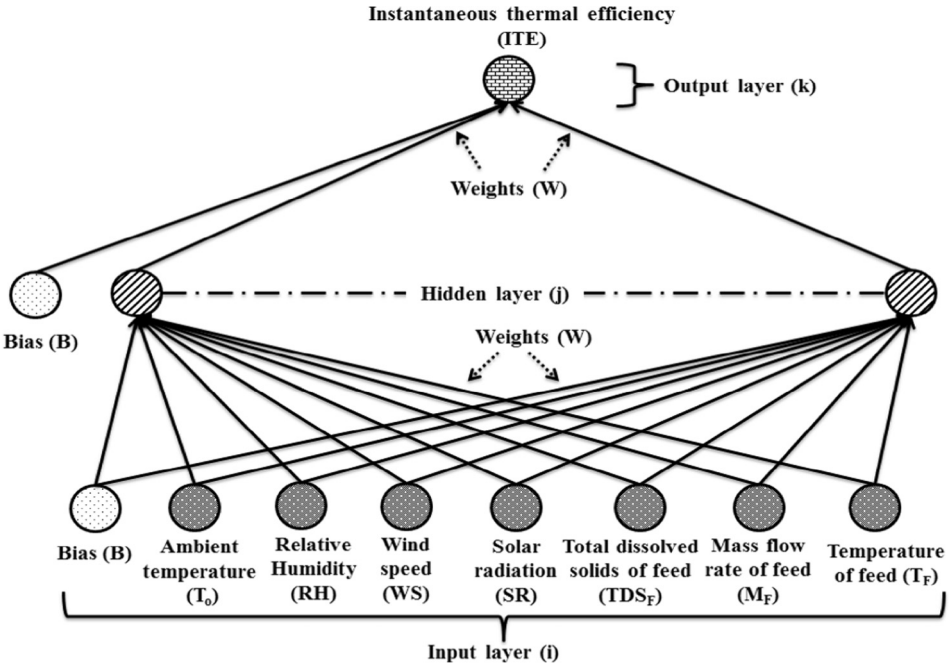

Fig. 2. Architecture of the ANN model used to predict the instantaneous thermal efficiency (ITE).

2.4. Multiple linear regression (MLR)

MLR analysis was first presented by Sir Francis Galton in the latter part of the 19th century. In this study, MLR analysis was used to model the relationship between two or more independent variables and a dependent (response) variable by fitting a linear equation to the observed data. The MLR model can be formulated as follows (Perers, 1997):

$$Y = \beta_o + \beta_1 x_1 + \beta_2 x_2 + \beta_3 x_3 \ldots \beta_n x_n \quad (6)$$

where Y is the output value (ITE); β_i (i = 0, . . . , n) are the regression coefficients, and Xi (i = 1, . . . , n) are the input parameters. The aim of MLR is to obtain an approximation function for the forecast future response of the system output. In MLR modeling, a dependent parameter is expressed as a linear combination of independent parameters and an intercept. In order to judge whether the best-fitting line fits the data to a satisfactory degree, this researcher studied the standard error of the coefficients (SE), t statistic (t-stat), and probability value (p-value) of the independent parameters. The MLR model was developed by using the same division of data points used with the ANN model (70% of the date points for training, 20% for testing and 10% for validation). This study utilized the IBM SPSS statistics 22 software package in the modeling process of MLR.

2.5. Models Evaluation using key performance indicators (KPIs)

The agreement between the observed data and predicted data for all models was computed through five KPIs, which were used to evaluate the performance of the developed models, as well as the goodness of fit and prediction accuracy. The five KPIs comprised the were the coefficient of determination (CD), root mean square error (RMSE), Chi-square (CS), coefficient of residual mass (CRM), model efficiency (ME), and mean absolute error (MAE). The KPIs can be defined and computed as follows:

The CD is the primary criterion for choosing the most suitable model to predict the ITE values. The CD can be used to test the linear relation between observed and predicted values and reveals the proportion of the total variance in the observed data that can be demonstrated by the developed model. The CD is computed as follows (Miehle et al., 2006):

$$CD = \frac{\left(\sum_{i=1}^{n}(ITE_{o,i} - \overline{ITE_o})(ITE_{p,i} - \overline{ITE_p})\right)^2}{\sum_{i=1}^{n}(ITE_{o,i} - \overline{ITE_o})^2 \times \sum_{i=1}^{n}(ITE_{p,i} - \overline{ITE_p})^2}, [0 \leqslant CD \leqslant 1] \quad (7)$$

The RMSE is a numerical indicator of precision and reliability for developed models. RMSE describes the difference between the observed and predicted values in the unit of the variable. RMSE = 0 indicates that there is no difference between model predictions and experimental observations. RMSE is calculated as follows (Miehle et al., 2006):

$$RMSE = \sqrt{\frac{\sum_{i=1}^{n}(ITE_{o,i} - ITE_{p,i})^2}{n}}, [0 \leqslant RMSE < \infty] \quad (8)$$

The ME is used to assess the predictive power of the ITE model. The closer the ME is to 1, the more accurate the model is. ME < 0 happens when the observed mean is a better predictor than the model. The ME is expressed as follows (Nash and Sutcliffe, 1970):

$$ME = 1 - \frac{\sum_{i=1}^{n}(ITE_{o,i} - ITE_{p,i})^2}{\sum_{i=1}^{n}(ITE_{o,i} - \overline{ITE_o})^2}, [-\infty < ME \leqslant 1] \quad (9)$$

The CS is a statistical measure of difference between observed values and predicted values to test the closeness of fit between them. The lower the value of the CS, the better the goodness of fit. The CS is estimated as follows (Boulinguiez et al., 2008):

$$CS = \sum_{i=1}^{n}\left[\frac{(ITE_{o,i} - ITE_{p,i})^2}{ITE_{p,i}}\right], [0 \leqslant CS < \infty] \quad (10)$$

The CRM is a statistical measure of the tendency of the model to over-predict or under-predict the measurements. Positive values of CRM indicate that the model over-predicts the measurements, while negative values of CRM show a tendency to under-predict the measurements. The CRM is found as follows (Loague and Green, 1991):

$$CRM = \frac{\left(\sum_{i=1}^{n} ITE_{p,i} - \sum_{i=1}^{n} ITE_{o,i}\right)}{\sum_{i=1}^{n} ITE_{o,i}}, [-\infty < CRM < \infty] \quad (11)$$

The MAE denotes the most absolute and relative meaningful measure of the model's error and ranges from 0 to 1, with lower values indicating better performance. The MAE is obtained as follows (Miehle et al., 2006):

$$MAE = \frac{\sum_{i=1}^{n} \left| ITE_{o,i} - ITE_{p,i} \right|}{n}, [0 \leqslant MAE \leqslant 1] \quad (12)$$

where $ITE_{o,i}$ = observed value; $ITE_{p,i}$ = predicted value; n = number of observations; $\overline{ITE_o}$ = averaged observed values; and $\overline{ITE_p}$ = averaged predicted values.

3. Results and discussion

3.1. Descriptive statistics and ITE characteristics

A sample of the data used in the current study is shown in Table 1. Additionally, Table 2 shows the average (AVG), minimum (MIN), maximum (MAX), standard deviation (SD), coefficient of variation (CV), skewness (SK), kurtosis (KR) of metrological and operational parameters used to develop the ITE forecast models. Table 2 shown that there was little variability in the sample distributions of the parameters employed in this investigation to develop the ITE forecast models, demonstrating that their values were all normally distributed to some extent. Fig. 3 also illustrates the scatter plot matrices presenting interrelations between the input parameters and ITE. This figure revealed the dependencies between the ITE and input parameters; however, the existing patterns and trends seem to be relatively complex and problematic. In added words, though variation in change of ITE seems to be depended on the changes in the other studied characteristics, the nature of the relationships is not easily comprehensible. Notwithstanding, it appears that the investigated meteorological and operational attributes may directly or indirectly affect the ITE and therefore ANN might be beneficial to be used to derive the functions translating such data into forecasts of ITE. However, the AVG, MIN, MAX, and SD of ITE were 55.62%, 29.64%, 70.28, and 9.35%, respectively. The SR was varied from 223.19 to 810.05 W/m^2 with a CV of 0.21 and T_o have AVG, MIN, and MAX values of 32.95, 24.30, and 39.36 °C, respectively. The distribution curves for all independent and dependent parameters are platykurtic since all KR values are less than 3. The distribution is highly skewed for SR (SK > 1), moderately skewed for T_o, T_F, TDS_F, and M_F (−1 < SK < −0.5 or 0.5 < SK < +1) and approximately symmetric for RH, WS and ITE (−0.5 < SK < 0.5). From the CV values, it is clear that the data of T_F and M_F are homogenous (CV < 0.10). T_o and ITE are relative homogenous ($0.10 \leqslant CV < 0.20$) and SR is relative heterogeneous ($0.20 \leqslant CV < 0.30$). The data of RH, WS, and TDS_F are heterogeneous (CV > 0.30). Generally, from the experimental results, the ITE increased progressively from the sunrise time until it reaches to maximum value about at noon and then declined till reached to the minimum value at sunset time. This means that the ITE tends to increase as SR increases and tends to decrease as SR decreases. This result agrees with those of Singh et al. (1995) and Afrand et al. (2010). MF and WS are found to be negatively correlated with ITE with a correlation coefficient (CC) = −0.55 and −0.40, respectively. These findings are consistent with the studies of Yadav and Kumar (1991) and Mashaly et al. (2015a). Also, the ITE were correlated well with T_o, RH, T_F and TDS_F by CC = 0.29, 0.21, 0.29 and 0.32, respectively. A more complete representation and detailed discussion of these experimental data can be found in Mashaly et al. (2015a).

3.2. ANN model architecture

Besides choosing the input parameters affecting the performance of the ANN model, it is important to determine the optimum architecture of the ANN model, in other words, the number of hidden neurons, and identifying the best activation/transfer function between neurons. Determining the number of neurons in the input and output layers is usually a simple process, since it is determined by the number of inputs and outputs, and the choice of input parameters is typically based on the nature of the problem. In contrast, determining the optimum architecture of the ANN model, especially selecting the number of neurons in the hidden layer, is one of the most important and difficult tasks (Baziar and Ghorbani, 2011). In this study, the optimal architecture was specified by changing the number of hidden nodes from two to ten and electing the ANN architecture that leads to the best findings. The ANN training process was stopped when maximum iterations of 50,000 were reached. A learn rate coefficient of 0.01 and a momentum factor of 0.80 were used. Moreover, the ANN model was run with different activation functions that include SIG and TANH. However, the optimum ANN architecture was selected through a trial-and-error method based on the statistical parameters of CD, RMSE, MAE, ME, CRM, and CS, all of which are numerical indicators used to assess the performance of the ANN architecture, as illustrated in Fig. 4.

Overall, for SIG function, the ANN architectures' CD values ranged from 0.942 to 0.957, ME values from 0.942 to 0.957, RMSE values from 1.819% to 2.138%, MAE values from 1.422% to 1.600%, CRM values from −6.55E−04 to 4.48E−05, and CS values from 2.428% to 3.548%. For the TANH function, the ANN architectures' DC values ranged from 0.963 to 0.984, ME values from 0.963 to 0.984, RMSE values from 1.131% to 1.458%, MAE values from 0.963% to 1.204%, CRM values from 2.07E−05 to 4.91E−04, and CS values from 0.956% to 1.542%. The tiny deviations between the observed and predicted results; as indicated in the values of the statistical indicators for both activation functions, in turn highlight the effectiveness of the ANN technique in the prediction

Table 1
Sample of input and output variables used for training the models for one operation day.

Date	Time	Inputs							Output
		To (°C)	RH (%)	WS (km/h)	SR (W/m^2)	T_F (°C)	M_F (L/min)	TDS_F (PPT)	ITE (%)
08/10/2013	9 AM	24.812	19.952	1.371	621.119	30.779	0.176	18.267	38.371
	10 AM	26.208	17.317	4.065	719.444	34.546	0.177	18.383	54.448
	11 AM	27.748	14.778	4.500	783.016	36.003	0.177	19.067	54.578
	12 PM	29.343	12.984	2.948	771.175	36.970	0.178	19.957	52.824
	1 PM	30.332	12.270	3.581	686.222	37.690	0.180	21.233	47.658
	2 PM	30.756	11.984	3.584	536.683	37.259	0.179	22.367	41.699
	3 PM	30.787	11.526	3.245	425.627	37.158	0.178	23.631	37.787

T_o: ambient temperature; RH: relative humidity; WS: wind speed; SR: solar radiation; T_F: feed temperature; M_F: feed flow rate; TDS_F: total dissolved solids of feed; ITE: instantaneous thermal efficiency.

Table 2
Statistical characteristics of the data used for the modeling process.

Parameter	Descriptive statistics						
	AVG	MIN	MAX	SD	CV	KUR	SKW
T_o (°C)	32.95	24.30	39.36	4.28	0.13	−0.96	0.07
RH (%)	13.88	7.81	30.19	6.16	0.44	0.35	1.14
WS (km/h)	1.39	0.00	5.18	1.56	1.12	−0.16	1.09
SR (W/m^2)	665.42	223.19	810.05	137.85	0.21	1.38	−1.29
T_F (°C)	37.99	29.39	42.75	2.81	0.07	0.58	−0.13
M_F (L/min)	0.17	0.16	0.18	0.00	0.03	0.68	−1.40
TDS_F (PPT)	28.14	4.71	99.43	25.69	0.91	0.87	1.36
ITE (%)	55.62	29.64	70.28	9.35	0.17	−0.19	−0.46

AVG: average value; MIN: minimum value; MAX: maximum value; SD: standard deviation; CV: coefficient of variation; KUR: kurtosis; SKW: skewness; T_o: ambient temperature; RH: relative humidity; WS: wind speed; SR: solar radiation; T_F: feed temperature; M_F: feed flow rate; TDS_F: total dissolved solids of feed; ITE: instantaneous thermal efficiency.

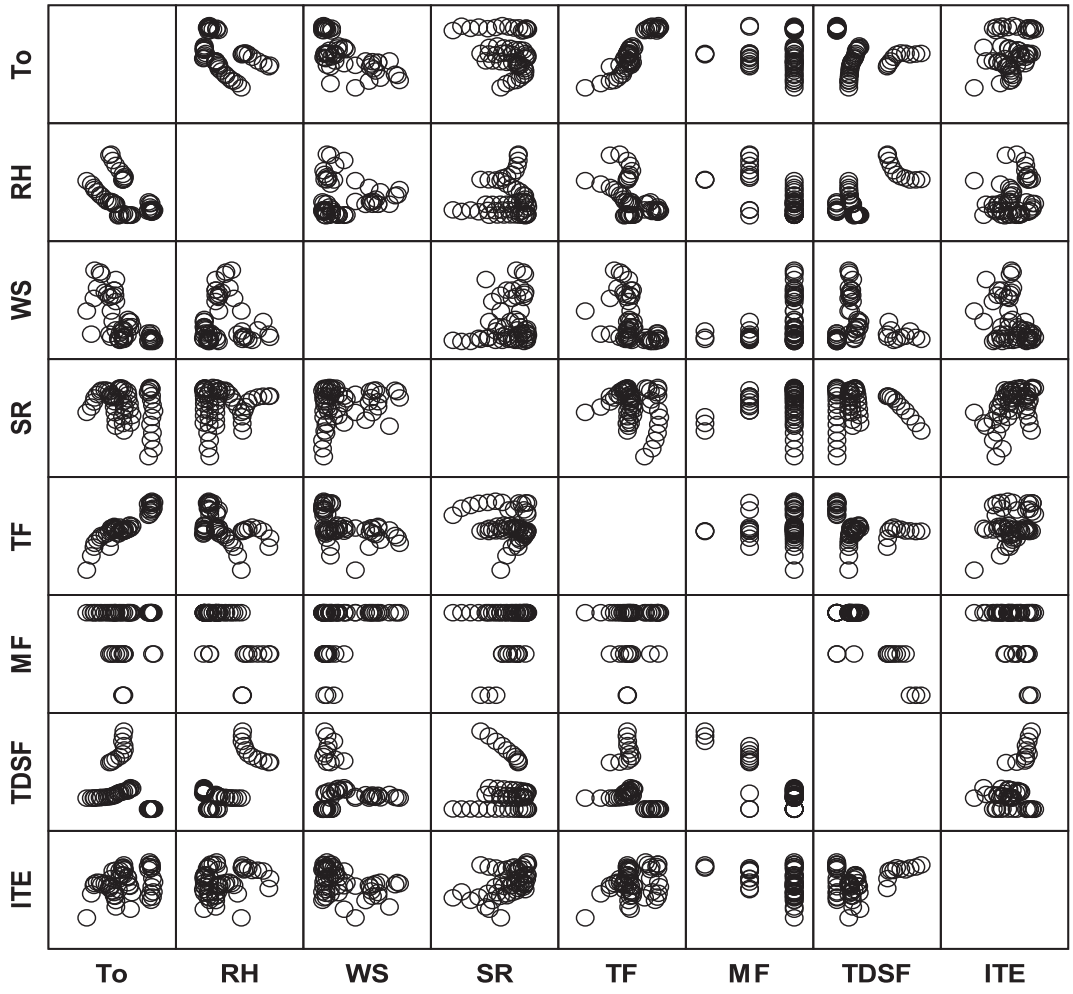

Fig. 3. Scatterplot matrix for the input and output variables (T_o: ambient temperature; RH: relative humidity; WS: wind speed; SR: solar radiation; T_F: feed temperature; M_F: feed flow rate; TDS_F: total dissolved solids of feed; ITE: instantaneous thermal efficiency).

process of ITE. This agrees with the findings of Tripathy and Kumar (2009), Porrazzo et al. (2013), Mashaly et al. (2015c), and Cao et al. (2016). However, the performance of the ANN architectures with the TANH function was better than that with the SIG function.

Moreover, the aforementioned statistical parameters were observed as the number of neurons in the hidden layer was increased. The ANN architecture improved with more neurons, as reflected in the values of the statistical parameters, especially for the TANH function as presented in Fig. 4. High values of CD and ME and low values of RMSE, MAE, CRM, and CS, all of which show good model performance, were obtained by increasing the number of hidden neurons to more than 2. For the SIG function, increasing the number of hidden neurons did not lead to a significant positive change in the performance, but sometimes led to a minute impairment in the performance. For instance, increasing the number of hidden neurons from 2 to 4, decreased the CD and ME values by 0.89% and 0.89%, respectively, and increased the RMSE, MAE, CRM, and CS values by 9.69%, 10.83%, 375.48%, and 29.01%, respectively. When the number of neurons in the hidden layer reached 6, impairment was observed in the ANN architecture due to using the

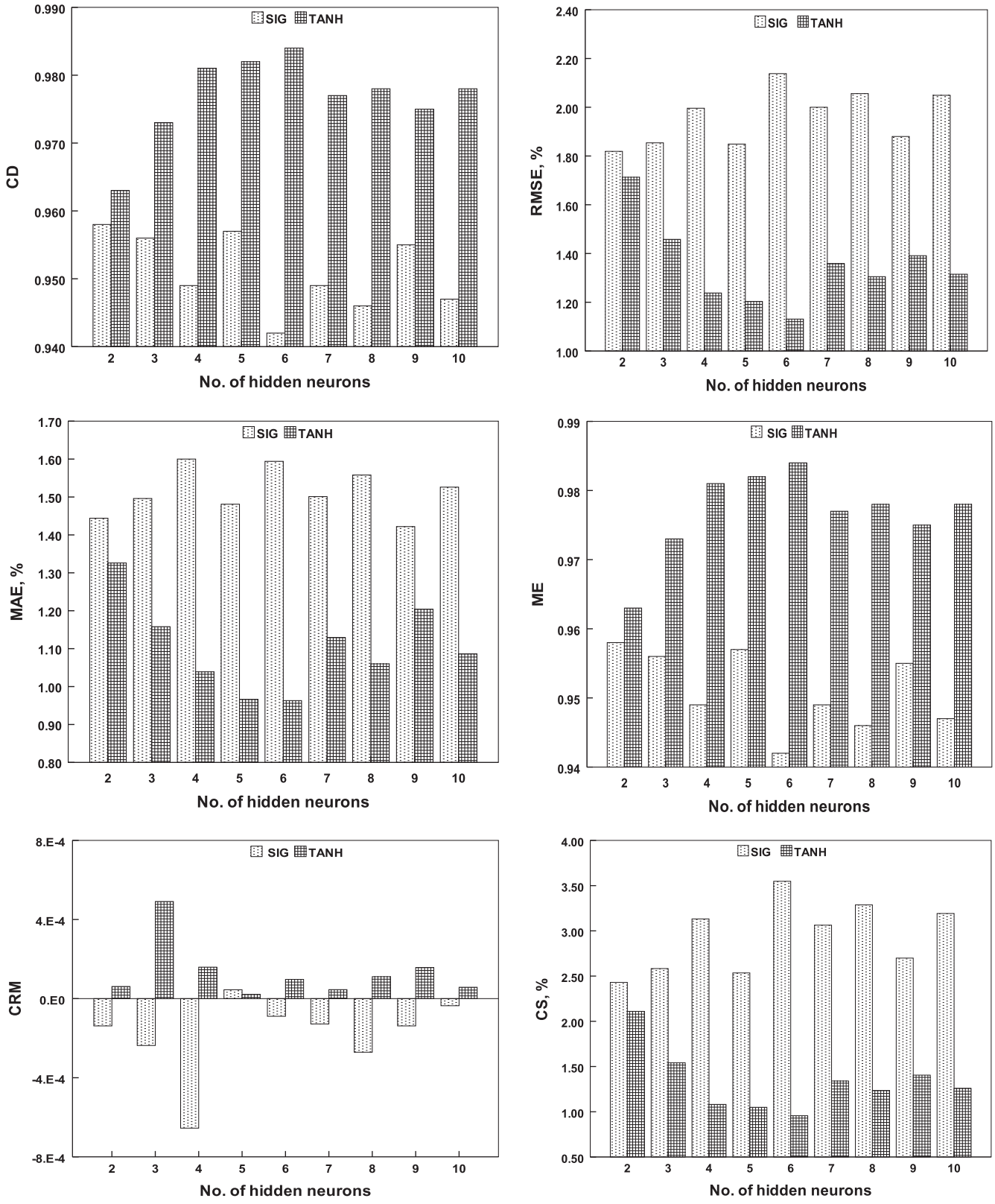

Fig. 4. Statistical performance of the ANN model for ITE with various transfer functions and hidden neurons during the training process.

SIG function (Fig. 4). Increasing the number of neurons in the hidden layer to above 6 impaired the ANN performance as demonstrated in Fig. 4. There was a fluctuation in the performance after the number of hidden neurons was increased to above 6, but in all the cases, the performance was less accurate than that of the TANH function.

On the other hand, Fig. 4 indicates that increasing the number of hidden neurons from 2 to 4 led to a noticeable enhancement in the ANN performance using the TANH function. The CD and ME values increased by 1.85% and 1.85%, respectively, and the RMSE and MAE values decreased by 27.70% and 21.66%, respectively. While the CRM value increased by 159.70%, but it was still very close to zero, the CS value decreased by 48.74% and came very close to zero. As noted in Fig. 4, the TANH function gave the best ANN performance for ITE. It is obvious that the developed ANN model with 6 hidden neurons and with an activation function of TANH has the minimal RMSE, MAE, CRM and CS, and maximal CD and ME. Also, the ANN model has presented more accurate forecasting than other ANN architectures. The CD value at this architecture was 0.984, and the ME was also 0.984. The RMSE and MAE were 1.131% and 0.963%, respectively. The CRM and CS values were 9.72E−05 and 0.956%, respectively. Increasing the number of neurons in the hidden layer above 6 slightly impaired the ANN performance, as displayed in Fig. 4. The contribution ratio of the input parameters for this architecture (7 input– 6 hidden neurons–1 output) revealed that the highest contribution values (23.58% and 22.33%) belonged to SR and T_o, respectively, which thus indicates that SR and T_o have the highest impact on ITE. This result was in agreement with the findings of Medugu and Ndatuwong (2009) and Rahbar and Esfahani (2012). The WS and M_F are minor contributors to ITE, contributing only 6.31% and 5.66%, respectively. The RH, T_F, and TDS_F were found to have a moderate influence on the ITE with a contribution ratio of 14.43%, 17.60%, and 10.09%, respectively.

Based on the above results, the most appropriate ANN architecture is 7–6–1 with the TANH function. This gave the best prediction of ITE with the minimum RMSE, MAE, CRM and CS, and the maximum CD and ME. The developed ANN model can be easily solved using a spreadsheet (i.e. Microsoft Excel). The developed model for ITE can be expressed by an algebraic system of equations:

$$ITE = \frac{1 - \exp\left[(-4.03 \times F_1 + 0.30 \times F_2 + 4.65 \times F_3 + 5.73 \times F_4 + 1.80 \times F_5 - 4.13F_6) - 0.30\right]}{1 + \exp\left[(-4.03 \times F_1 + 0.30 \times F_2 + 4.65 \times F_3 + 5.73 \times F_4 + 1.80 \times F_5 - 4.13F_6) - 0.30\right]} \quad (13)$$

where F_1, F_2, F_3, F_4, F_5 *and* F_6 are computed as follows:

$$F_1 = \frac{1 - \exp[(-1.07 \times T_o - 4.88 \times RH + 1.43 \times WS - 1.12 \times SR + 2.01 \times T_F - 0.12 \times M_F + 0.75 \times TDS_F) + 0.24]}{1 + \exp[(-1.07 \times T_o - 4.88 \times RH + 1.43 \times WS - 1.12 \times SR + 2.01 \times T_F - 0.12 \times M_F + 0.75 \times TDS_F) + 0.24]} \quad (14)$$

$$F_2 = \frac{1 - \exp[(-0.48 \times T_o - 0.35 \times RH + 0.13 \times WS - 0.26 \times SR + 0.34 \times T_F + 0.30 \times M_F - 0.15 \times TDS_F) + 0.33]}{1 + \exp[(-0.48 \times T_o - 0.35 \times RH + 0.13 \times WS - 0.26 \times SR + 0.34 \times T_F + 0.30 \times M_F - 0.15 \times TDS_F) + 0.33]} \quad (15)$$

$$F_3 = \frac{1 - \exp[(1.20 \times T_o - 2.84 \times RH + 1.83 \times WS - 0.42 \times SR - 1.27 \times T_F - 0.82 \times M_F + 3.14 \times TDS_F) + 1.62]}{1 + \exp[(1.20 \times T_o - 2.84 \times RH + 1.83 \times WS - 0.42 \times SR - 1.27 \times T_F - 0.82 \times M_F + 3.14 \times TDS_F) + 1.62]} \quad (16)$$

$$F_4 = \frac{1 - \exp[(3.14 \times T_o - 4.61 \times RH - 1.86 \times WS - 1.43 \times SR - 0.28 \times T_F + 3.24 \times M_F - 3.36 \times TDS_F) - 2.09]}{1 + \exp[(3.14 \times T_o - 4.61 \times RH - 1.86 \times WS - 1.43 \times SR - 0.28 \times T_F + 3.24 \times M_F - 3.36 \times TDS_F) - 2.09]} \quad (17)$$

$$F_5 = \frac{1 - \exp[(1.88 \times T_o + 2.13 \times RH + 0.52 \times WS + 0.75 \times SR - 0.55 \times T_F - 0.42 \times M_F - 0.11 \times TDS_F) + 0.81]}{1 + \exp[(1.88 \times T_o + 2.13 \times RH + 0.52 \times WS + 0.75 \times SR - 0.55 \times T_F - 0.42 \times M_F - 0.11 \times TDS_F) + 0.81]} \quad (18)$$

$$F_6 = \frac{1 - \exp[(1.49 \times T_o - 3.42 \times RH - 2.04 \times WS - 6.37 \times SR - 0.20 \times T_F + 2.97 \times M_F - 1.50 \times TDS_F) + 1.81]}{1 + \exp[(1.49 \times T_o - 3.42 \times RH - 2.04 \times WS - 6.37 \times SR - 0.20 \times T_F + 2.97 \times M_F - 1.50 \times TDS_F) + 1.81]} \quad (19)$$

3.3. MLR model

The MLR model was carried out to correlate the observed ITE to seven variables, namely, T_o, RH, WS, SR, T_F, M_F, and TDS_F. For this purpose, the MLR model was generated using IBM SPSS statistics 22 as mentioned before. Also, the MLR model was applied to the same inputs and output data which used for the ANN model. The following equation is achieved for the computation of ITE based on the MLR model:

$$ITE = 81.14 + 1.90T_o + 0.35RH + 0.01WS + 0.05RS - 1.18T_F - 470.94M_F + 0.06TDS_F \quad (20)$$

The MLR model based equation (Eq. (20)) allows us to evaluate the rate of variations of ITE with changes in each of its influential meteorological and operational variables (i.e., T_o, RH, WS, SR, T_F, M_F, and TDS_F) and thus provides insight into the physics of the problem. This can be done simply by taking the derivative of ITE in Eq. (20) with respect to each of its independent variables. It helps us understand how ITE varies with T_o, RH, WS, SR, T_F, M_F, and TDS_F and to what extent these variables should be changed to reach the appropriate ITE value. The SE of regression coefficients, t-stat and p-value of independent variables (T_o, RH, WS, SR, T_F, M_F and TDS_F) are presented in Table 3. The MLR model showed that all independent variables were directly proportional to ITE. The SE determines the accuracy of the estimate of the coefficient. The smaller the SE, the more accurate the estimate. Based on the results in Table 3, the SE of the SR (0.01) is the smallest. The significance of each coefficient of the obtained MLR model was determined by t-stat and p-value, which are displayed in Table 3. The larger the t-stat and the smaller the p-value, the more significant is the corresponding coefficient. The absolute value of the t-stat should be greater than the critical t-value. The t-stat value of SR is greater than 2.040 (critical t-value at 31 degrees of freedom) which indicates the accuracy of the coefficient of this variable. From Table 3, the meaningfulness degrees of input parameters of the MLR model can be determined through the value of p-value being less than the significance level α (0.05). By examining the p-value values, it was shown that there is a significant relationship between only SR and ITE. On the other hand, the other parameters were not statistically significant as p-value is greater than 0.05. Thus, SR is the most significant variable in the MLR model with the highest t-stat and smallest p-value. This agrees with the results of Chaouchi et al. (2007) and Liu et al. (2015).

Table 3
Standard error (SE) of regression coefficients, t statistic (t-stat), and probability (p-value) of the MLR model parameters.

Dependent parameter		Independent parameters							
		Intercept	T_o	RH	WS	SR	T_F	M_F	TDS_F
ITE	SE	62.10	0.99	0.23	0.97	0.01	1.23	285.73	0.06
	t-stat	1.31	1.91	1.51	0.01	8.33	−0.94	−1.65	0.96
	p-value	0.20	0.07	0.14	0.99	0.00	0.35	0.11	0.35

T_o: ambient temperature; RH: relative humidity; WS: wind speed; SR: solar radiation; T_F: feed temperature; M_F: feed flow rate; TDS_F: total dissolved solids of feed; ITE: instantaneous thermal efficiency.

3.4. Comparison between the developed ANN and MLR models

To further assess the capability of ANN and MLR models in estimating ITE, their results are compared. The comparison of the observed ITE values versus the predicted ITE values for the training, testing and validation datasets for the ANN and MLR models is shown in Fig. 5. The performance of the ANN and MLR models was also evaluated using the statistical parameters given in Table 3. For the ANN model, the tight banding around the 1:1 line demonstrates noteworthy agreement between the predicted and observed ITE values, as indicated in Fig. 4 using the training dataset. The values obtained using the ANN model were: CD of 0.984, RMSE of 1.130%, MAE of 0.962%, ME of 0.984, CRM of 0.004, and CS of 0.955 (Table 4). Thus, the CD and ME values are very close to one, while the RMSE, MAE, CRM, and CS values are close to zero, showing an excellent agreement between the observed and predicted ITE values. For the MLR model, many points are located above and below the 1:1 line during the training period. Moreover, the CD and ME were decreased by almost 18.902% and 19.614%, respectively, and the RMSE, MAE, CRM, and CS values were increased by about 259.381%, 223.493%, 14468.158%, and 1155.183%, respectively, using the MLR model during the training period (Table 4). As shown in Fig. 5, the box-plot (right panel) was used to compare the observed and predicted values for both models. Actually, one of the most important characteristics of the developed models in predicting ITE is keeping the fundamental statistics of the observed values, such as the minimum value, maximum value, median value, upper quartile value, and lower quartile value. The box-plot is a convenient way to depict graphically showing groups of numerical data through their five-number summaries: the minimum value, lower quartile value, median value, upper quartile value, and maximum value. The lower and upper lines of the boxes give the lower quartile and upper quartile values, and the whiskers above and below the box show the locations of the minimum and maximum values. The middle line of the box gives the median value. For the training period, the box-plot presented in Fig. 5 shows that the ANN model is capable of retaining the minimum, maximum, median, upper, and lower quartile statistics of the observed values. Thus, there is no significant difference between the observed values and the predicted values in the ANN model and they have the same median value and the same distribution. Therefore, the ANN model performed better than the MLR model in conserving the fundamental statistics of the observed values of ITE, and it is the more accurate than the MLR model. Fig. 6 shows the relative errors of the predicted ITE values for the ANN model and the MLR model. Using the training dataset, the relative errors of the predicted ITE values are mostly in the domain range of −6 to +8% for the ANN model; for the MLR model, the domain ranges from −15% to +35%. The low relative errors support the accuracy of the developed ANN model. Furthermore, Fig. 5 depicts the relationship between the observed and predicted ITE values of ITE using the ANN and MLR models during the testing period. As seen, there is good agreement between the observed and predicted values for the ANN model. This is revealed by the lower values of RMSE (2.070%), MAE (1.659%), CRM (−0.006), and CS (0.867%), which were all close to zero, while the CD (0.943) and ME (0.933) values were close to one (Table 4). However, as shown in Fig. 5, many of the points given by the MLR model are located above and below the 1:1 line during the testing period. Moreover, the MLR model had a CD value that was about 23% less accurate than the CD value obtained from the ANN model during the testing period. The RMSE and MAE values for the MLR model (4.215% and 3.193%, respectively) were almost double that of the corresponding values for the ANN model. The ME value for the MLR model was about 22.51% less accurate than the ME for the ANN model. The CRM value (+0.001) refers to over-prediction, but it is small; and, the CS value for the MLR model was almost four-times that of the CS value for the ANN model. As in the training and testing periods, the ANN model gives better agreement between the observed and predicted values than the MLR model in the validation period (Fig. 5). The CD value for the ANN model was 0.921, which is about 24.7% more accurate than the CD value for the MLR model. The RMSE value from the ANN model was 2.600, which is about half the RMSE value obtained using the MLR model. The MAE value in the ANN model was 28.5% lower than the value obtained with the MLR model. The ME value for the ANN model was 0.882, which is closer to one than the ME value given by the MLR model, which was 0.605. The CRM value (−0.019) refers to an under-prediction, but it is small; and, the CS value for the ANN model was almost three-times less than the CS value for the MLR model. As shown in the box-plots in Fig. 5, there is a good agreement between the observed data and the ANN model; they have almost the same statistics. However, the predicted values in the MLR model varied during the testing and validation periods. Fig. 6 displays the relative errors of the predicted ITE values for the ANN and MLR models during the testing and validation periods, demonstrating the figure illustrates differences between the findings of the two models. In the MLR model, the relative errors ranged between −8.19% and +21.53% for the testing period, and between −12.68% and +19.09% for the validation period, respectively. The corresponding values for the developed ANN model were lower; they ranged from −5.16% to +9.77% and from −7.46% to +5.71% for the testing and validation periods, respectively. Overall, as demonstrated in the data presented in Table 4 and Figs. 5, 6, the ANN model is better than the MLR model. This is in agreement with the findings reported by Şahin et al. (2013), Mashaly and Alazba (2016b) and Yadav and Chandel (2017).

4. Conclusion

In this study, ANN and MLR models were used to forecast the ITE of an inclined passive solar still in arid climate. The ITE is an important determinant of the effectiveness and performance of solar stills. The AWD was used as a feed-water source in the experimental work. On the basis of a correlation analysis and previous studies, seven meteorological and operational variables, namely, T_o, RH, WS, SR, T_F, TDS_F, and M_F, were used for developing ANN and MLR models to predict the ITE. The models were trained,

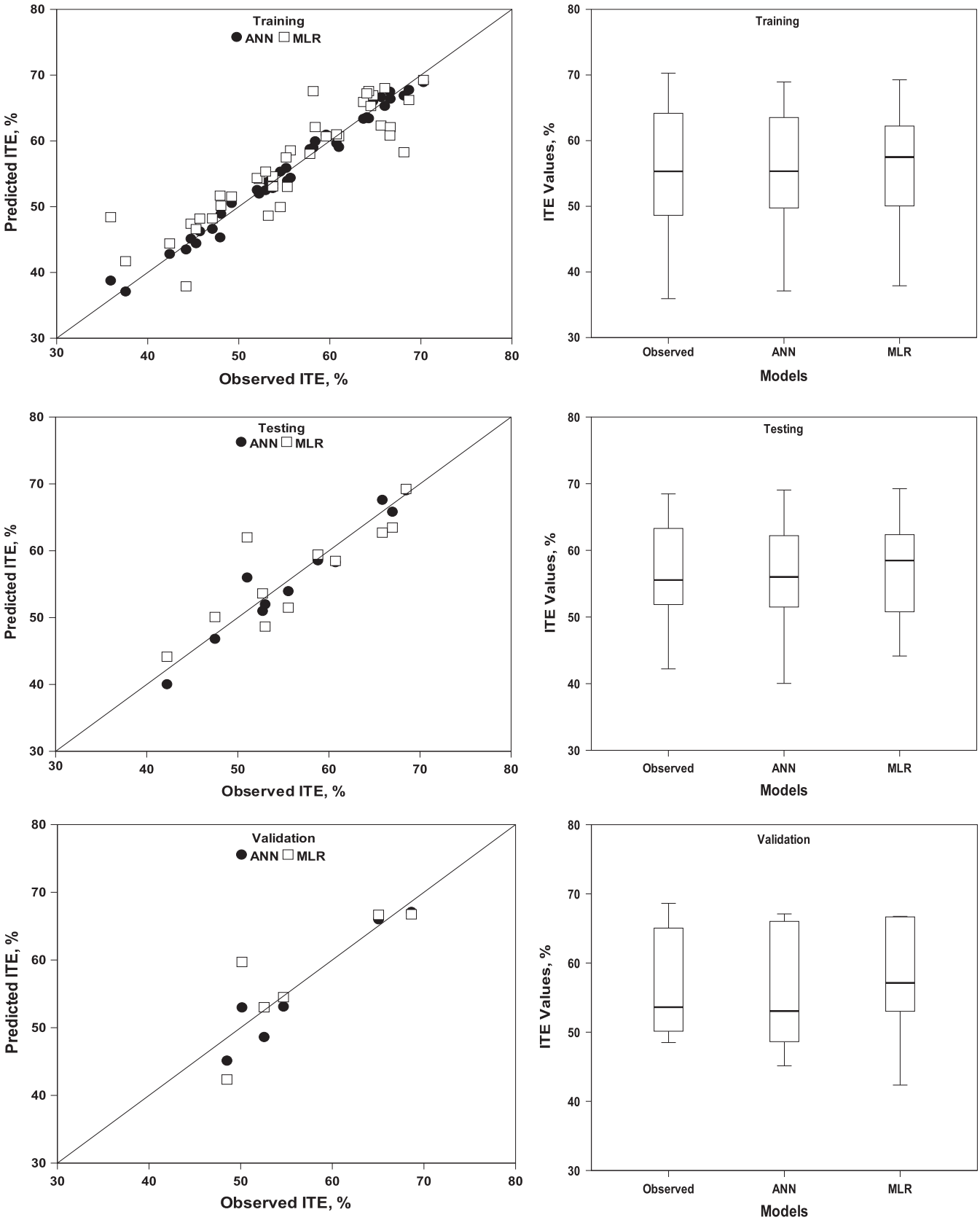

Fig. 5. Comparison between observed and predicted values of ITE using the ANN and MLR models during the training, testing and validation periods.

tested, and validated using data collected from the experimental work. The use of various transfer functions revealed that the optimal ANN model had a feed-forward back propagation architecture with 7–6–1 neurons and a hyperbolic tangent function in the hid-

Table 4
Statistical parameters for assessing the performance of the ANN and MLR models during training, testing, and validation periods.

	CD	RMSE	MAE	ME	CRM	CS
Training						
ANN	0.984	1.130	0.962	0.984	9.61E−05	0.955
MLR	0.798	4.061	3.112	0.791	0.014	11.987
Testing						
ANN	0.943	2.070	1.659	0.933	−0.006	0.867
MLR	0.726	4.215	3.193	0.723	0.001	3.339
Validation						
ANN	0.921	2.600	2.366	0.882	−0.019	0.816
MLR	0.694	4.758	3.308	0.605	0.010	2.525

CD: coefficient of determination; RMSE: root mean square error; MAE: mean absolute error; CRM: coefficient of residual mass; ME: model efficiency; CS: Chi-square.

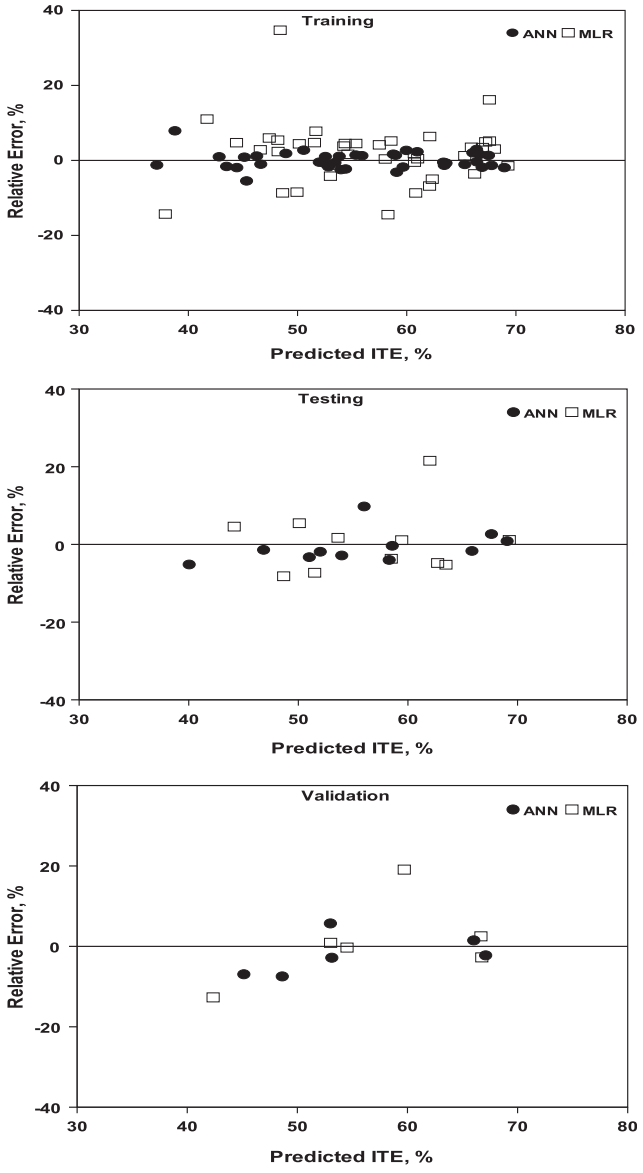

Fig. 6. Relative errors for the ANN model and the MLR model using the training, testing and validation data sets.

den and output layers. The performance of ANN and MLR models was assessed by comparing the predicted values for both models with the observed values by using various KPIs, namely CD, RMSE, CS, CRM, ME, and MAE. The results revealed that the ANN model can predict the ITE more accurately than the MLR model; moreover, compared with the MLR, the ANN model exhibited lower RMSE, MAE, CRM, and CS and higher CD and ME. The results indicated that the ANN model was more effective, reliable, and accurate for ITE prediction than the MLR model. With respect to the time and costs involved infield experiments, by using the ANN model, acceptable findings can be forecasted rather than measured, thereby reducing the costs, efforts, and time required. Thus, the use of the ANN model can minimize losses in terms of the required time, materials, efforts, and costs. Therefore, this study is useful for the design and optimization of solar stills in practice.

Conflicts of interest

The authors declare no conflict of interest.

Acknowledgement

The project was financially supported by King Saud University, Vice Deanship of Research Chairs.

References

Abbas, A., Al-Bastaki, N., 2005. Modeling of an RO water desalination unit using neural networks. Chem. Eng. J. 114 (1), 139–143.
Abderachid, T., Abdenacer, K., 2013. Effect of orientation on the performance of a symmetric solar still with a double effect solar still (comparison study). Desalination 329, 68–77.
Abulnour, A.G., Sorour, M.H., Talaat, H.A., 2003. Comparative economics for desalting of agricultural drainage water (ADW). Desalination 152 (1–3), 353–357.
Afrand, M., Behzadmehr, A., Karimipour, A., 2010. A Numerical simulation of solar distillation for installation in Chabahar-Iran. World Acad. Sci. Eng. Technol. 47, 469–474.
Aish, A.M., Zaqoot, H.A., Abdeljawad, S.M., 2015. Artificial neural network approach for predicting reverse osmosis desalination plants performance in the Gaza Strip. Desalination 367, 240–247.
Arif, C., Mizoguchi, M., Setiawan, B.I., Doi, R., 2012. Estimation of soil moisture in paddy field using Artificial Neural Networks. Int. J. Adv. Res. Artif. Intell. (IJARAI) 1 (1), 17–21.
Ayoub, G.M., Malaeb, L., 2012. Developments in solar still desalination systems: a critical review. Crit. Rev. Env. Sci. Tec. 42 (19), 2078–2112.
Badran, O.O., Abu-Khader, M.M., 2007. Evaluating thermal performance of a single slope solar still. Heat Mass Transfer 43, 985–995.
Basheer, I.M., Hajmeer, M., 2000. Artificial neural networks: fundamentals, computing, design, and application. J. Microbiol. Methods 43, 3–31.
Baziar, M.H., Ghorbani, A., 2011. Evaluation of lateral spreading using artificial neural networks. Expert Syst. Appl. 38, 5958–5966.
Benli, H., 2013. Determination of thermal performance calculation of two different types solar air collectors with the use of artificial neural networks. Int. J. Heat Mass Tran. 60, 1–7.
Boulinguiez, B., Le Cloirec, P., Wolbert, D., 2008. Revisiting the determination of langmuir parameters application to tetrahydrothiophene adsorption onto activated carbon. Langmuir 24, 6420–6424.
Bourquin, J., Schmidli, H., Hoogevest, P., Leuenberger, H., 1998. Advantages of artificial neural networks (ANNs) as alternative modeling technique for data sets showing non-linear relationships using data from a galenical study on a solid dosage form. Eur. J. Pharm. Sci. 7, 5–16.
Çakmak, G., Yildiz, C., 2011. The prediction of seedy grape drying rate using a neural network method. Comput. Electron. Agr. 75 (1), 132–138.

Cao, W., Liu, Q., Wang, Y., Mujtaba, I.M., 2016. Modeling and simulation of VMD desalination process by ANN. Comput. Chem. Eng. 84, 96–103.
Chaouchi, B., Zrelli, A., Gabsi, S., 2007. Desalination of brackish water by means of a parabolic solar concentrator. Desalination 217 (1), 118–126.
Dursun, M., Özden, S., 2014. An efficient improved photovoltaic irrigation system with artificial neural network based modeling of soil moisture distribution – A case study in Turkey. Comput. Electron. Agric. 102, 120–126.
Fadare, D.A., 2009. Modelling of solar energy potential in Nigeria using an artificial neural network model. Appl. Energy 86 (9), 1410–1422.
Ferreira, P.M., Faria, E.A., Ruano, A.E., 2002. Neural network models in greenhouse air temperature prediction. Neurocomputing 43 (1–4), 51–75.
Goh, A.T.C., 1995. Back-propagation neural networks for modeling complex systems. Artif. Intell. Eng. 9, 143–151.
Gregory, P.J., 2012. Soils and food security: challenges and opportunities. In: Hester, R.E., Harrison, R.M. (Eds.), Soils and Food Security. RSC Publishing.
Haykin, S., 1999. Neural Networks: A Comprehensive Foundation. Prentice Hall, Upper Saddle River, New Jersey.
Kalogirou, S.A., 2006. Prediction of flat-plate collector performance parameters using artificial neural networks. Sol. Energy 80 (3), 248–259.
Kalogirou, S., Panteliou, S., Dentsoras, A., 1999a. Modeling of solar domestic water heating systems using artificial neural networks. Sol. Energy 65 (6), 335–342.
Kalogirou, S., Panteliou, S., Dentsoras, A., 1999b. Artificial neural networks used for the performance prediction of a thermosyphon solar water heater. Renew. Energ. 18, 87–99.
Khayet, M., Cojocaru, C., Essalhi, M., 2011. Artificial neural network modeling and response surface methodology of desalination by reverse osmosis. J. Membr. Sci. 368 (1–2), 202–214.
Lek, S., Guégan, J.F., 1999. Artificial neural networks as a tool in ecological modeling, an introduction. Ecol. Model. 120, 65–73.
Liu, X., Huang, J., Mao, Q., 2015. Sensitive analysis for the efficiency of a parabolic trough solar collector based on orthogonal experiment. Int. J. Photoenergy. http://dx.doi.org/10.1155/2015/151874.
Loague, K., Green, R.E., 1991. Statistical and graphical methods for evaluating solute transport models: overview and application. J. Contam. Hydrol. 7, 51–73.
Mashaly, A.F., Alazba, A.A., Al-Awaadh, A.M., 2015a. Assessing the performance of solar desalination system to approach near-ZLD under hyper arid environment. Desalin. Water Treat. 57, 12019–12036.
Mashaly, A.F., Alazba, A.A., Al-Awaadh, A.M., Mattar, M.A., 2015b. Predictive model for assessing and optimizing solar still performance using artificial neural network under hyper arid environment. Sol. Energy 118, 41–58.
Mashaly, A.F., Alazba, A.A., Al-Awaadh, A.M., Mattar, M.A., 2015c. Area determination of solar desalination system for irrigating crops in greenhouses using different quality feed water. Agr. Water Manage. 154, 1–10.
Mashaly, A.F., Alazba, A.A., 2016a. Comparison of ANN, MVR, and SWR models for computing thermal efficiency of a solar still. Int. J. Green Energy 13 (10), 1016–1025.
Mashaly, A.F., Alazba, A.A., 2016b. MLP and MLR models for instantaneous thermal efficiency prediction of solar still under hyper-arid environment. Comput. Electr. Agric. 122, 146–155.
Mashaly, A.F., Alazba, A.A., 2016c. Neural network approach for predicting solar still production using agricultural drainage as a feedwater source. Desalin. Water Treat. 57 (59), 28646–28660.
Mashaly, A.F., Alazba, A.A., 2017. Artificial intelligence for predicting solar still production and comparison with stepwise regression under arid climate. J. Water Supply Res. Technol.-Aqua 66 (3), 166–177.
Mashaly, A.F., Alazba, A.A., 2015. Comparative investigation of artificial neural networks learning algorithms for modeling solar still production. J. Water Reuse Desal. 5 (4), 480–493.
McCool, B.C., Rahardianto, A., Faria, J., Kovac, K., Lara, D., Cohen, Y., 2010. Feasibility of reverse osmosis desalination of brackish agricultural drainage water in the San Joaquin Valley. Desalination 261 (3), 240–250.
Medugu, D.W., Ndatuwong, L.G., 2009. Theoretical analysis of water distillation using solar still. Int. J. Phys. Sci. 4 (11), 705–712.
Miehle, P., Livesley, S.J., Liw, C., Feikemaz, P.M., Adams, M.A., Arndt, S.K., 2006. Quantifying uncertainty from large-scale model predictions of forest carbon dynamics. Glob. Chang. Biol. 12, 1421–1434.
Monowe, P., Masale, M., Nijegorodov, N., Vasilenko, V., 2011. A portable single-basin solar still with an external reflecting booster and an outside condenser. Desalination 280 (1), 332–338.
Nash, J.E., Sutcliffe, J.V., 1970. River flow forecasting through conceptual models, 1: a discussion of principles. J. Hydrol. 10, 282–290.
Omara, Z.M., Kabeel, A.E., 2014. The performance of different sand beds solar stills. Int. J. Green Energy 11 (3), 240–254.
Perers, B., 1997. An improved dynamic solar collector test method for determination of non-linear optical and thermal characteristics with multiple regression. Sol. Energy 59 (4–6), 163–178.
Porrazzo, R., Cipollina, A., Galluzzo, M., Micale, G., 2013. A neural network-based optimizing control system for a seawater-desalination solar-powered membrane distillation unit. Comput. Chem. Eng. 54, 79–96.
Rahbar, N., Esfahani, J.A., 2012. Experimental study of a novel portable solar still by utilizing the heatpipe and thermoelectric module. Desalination 284, 55–61.
Rai, S.N., Tiwari, G.N., 1983. Single basin solar still coupled with flat plate collector. Energ. Convers. Manage. 23 (3), 145–149.
Refalo, P., Ghirlando, R., Abela, S., 2016. The use of a solar chimney and condensers to enhance the productivity of a solar still. Desalin. Water Treat. 57 (48–49), 23024–23037.
Şahin, M., Kaya, Y., Uyar, M., 2013. Comparison of ANN and MLR models for estimating solar radiation in Turkey using NOAA/AVHRR data. Adv. Space Res. 51 (5), 891–904.
Sharon, H., Reddy, K.S., Krithika, D., Philip, L., 2017. Experimental performance investigation of tilted solar still with basin and wick for distillate quality and enviro-economic aspects. Desalination 410, 30–54.
Shukla, S.K., 2014. Application of solar distillation systems with phase change material storage. In: Modern Mechanical Engineering. Springer, Berlin Heidelberg, pp. 15–42.
Singh, A.K., Tiwari, G.N., Sharma, P.B., Emran, K., 1995. Optimization of orientation for higher yield of solar still for a given location. Energ. Convers. Manage. 36 (3), 175–187.
Singh, H.N., Tiwari, G.N., 2004. Monthly performance of passive and active solar stills for different Indian climatic conditions. Desalination 168, 145–150.
Sorour, M.H., El Defrawy, N.M.H., Shaalan, H.F., 2003. Treatment of agricultural drainage water via lagoon/reverse osmosis system. Desalination 152, 359–366.
Sorour, M.H., Abulnour, A.G., Talaat, H.A., 1992. Desalination of agricultural drainage water. Desalination 86 (1), 63–75.
Stuber, M.D., Sullivan, C., Kirk, S.A., Farrand, J.A., Schillaci, P.V., Fojtasek, B.D., Mandell, A.H., 2015. Pilot demonstration of concentrated solar-powered desalination of subsurface agricultural drainage water and other brackish groundwater sources. Desalination 355, 186–196.
Talaat, H.A., Ahmed, S.R., 2007. Treatment of agricultural drainage water: technological schemes and financial indicators. Desalination 204 (1–3), 102–112.
Tiwari, A.K., Tiwari, G.N., 2006. Effect of water depths on heat and mass transfer in a passive solar still: in summer climatic condition. Desalination 195 (1–3), 78–94.
Tiwari, G.N., 2006. Solar Energy Technology Advances. Nova Publishers.
Tripathi, R., Tiwari, G.N., 2005. Effect of water depth on internal heat and mass transfer for active solar distillation. Desalination 173 (2), 187–200.
Tripathy, P.P., Kumar, S., 2009. Neural network approach for food temperature prediction during solar drying. Int. J. Therm. Sci. 48 (7), 1452–1459.
Velmurugan, V., Pandiarajan, S., Guruparan, P., Subramanian, L.H., Prabaharan, C.D., Srithar, K., 2009. Integrated performance of stepped and single basin solar stills with mini solar pond. Desalination 249 (3), 902–909.
WWAP (United Nations World Water Assessment Programme), 2014. The United Nations World Water Development Report 2014: Water and Energy. Paris, UNESCO.
Yadav, A.K., Chandel, S.S., 2017. Identification of relevant input variables for prediction of 1-minute time-step photovoltaic module power using Artificial Neural Network and Multiple Linear Regression Models. Renew. Sustain. Energy Rev. http://dx.doi.org/10.1016/j.rser.2016.12.029.
Yadav, Y.P., Kumar, A., 1991. Transient analytical investigations on a single basin solar still with water flow in the basin. Energ. Convers. Manage. 31 (1), 27–38.